Supplementary Information (SI)

Regulating the Kinetic Behaviors of Polysulfides by Designing an Au-COF Interface in Lithium-Sulfur Batteries

Chan Li, Ke Yang, Zelin Ma, Fei Zhao, Juan Li, Xinwu Xu, Xiaoyu Hao, Haoyuan Qi, Yibo He*

State Key Laboratory of Solidification Processing, Center of Advanced Lubrication and Seal Materials, School of Materials Science and Engineering, Northwestern Polytechnical University, Youyi Road 127#, Xi'an 710072, Shaanxi, P. R. China.

*Corresponding author. E-mail: heyibo@nwpu.edu.cn

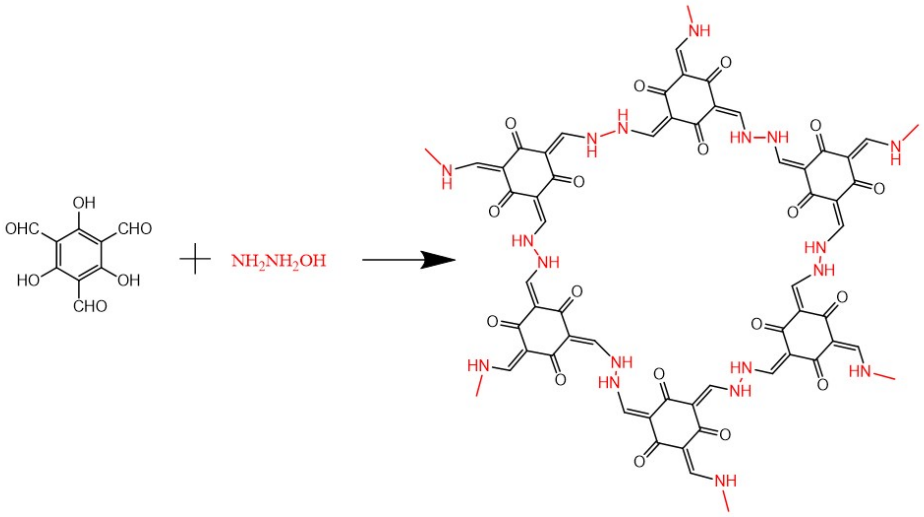

Fig. S1 Synthetic scheme of the NUS-2.

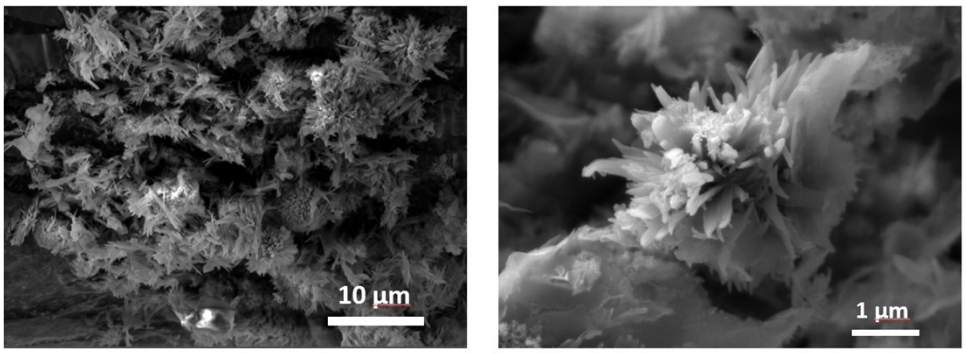

Fig. S2 SEM images of NUS-2 powder at different magnifications.

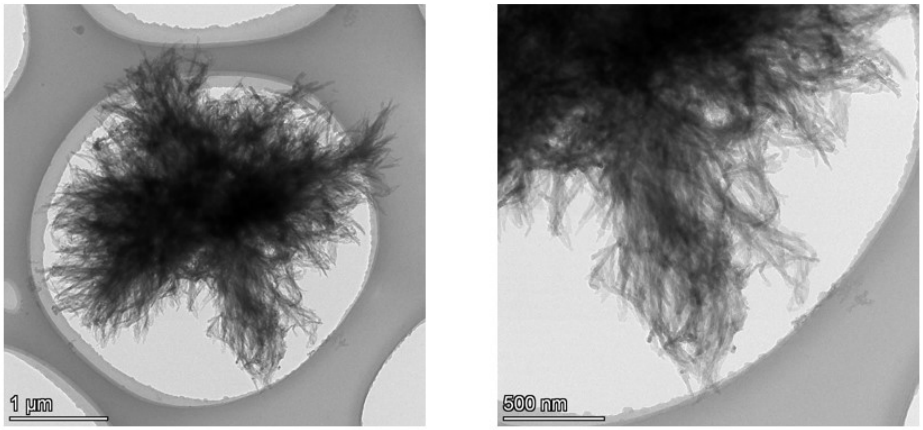

Fig. S3 TEM images of NUS-2 powder at different magnifications.

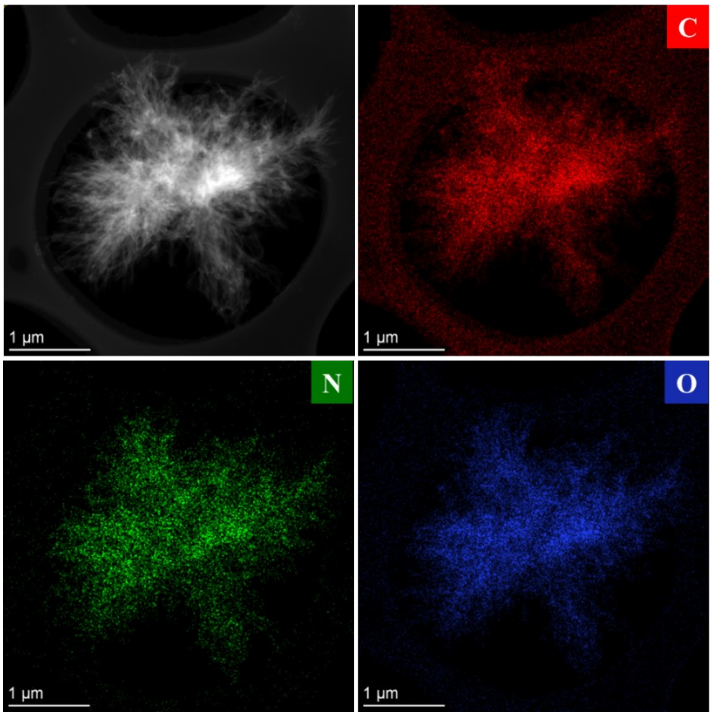

Fig. S4 TEM and corresponding elemental mapping images of NUS-2 powder.

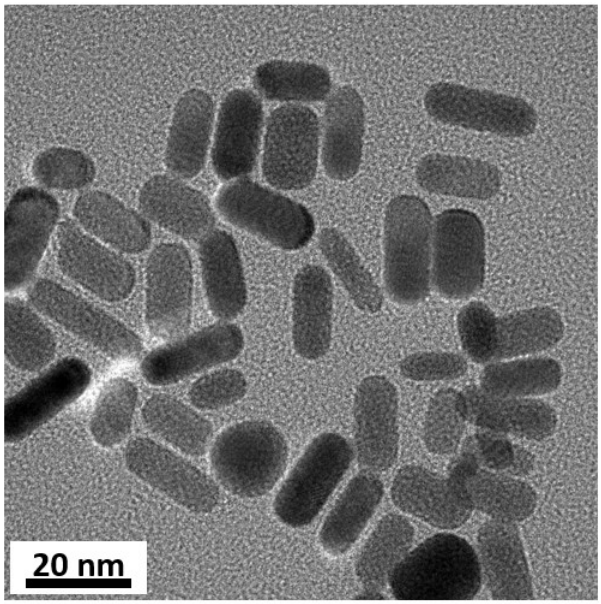

Fig. S5 TEM image of Au NPs.

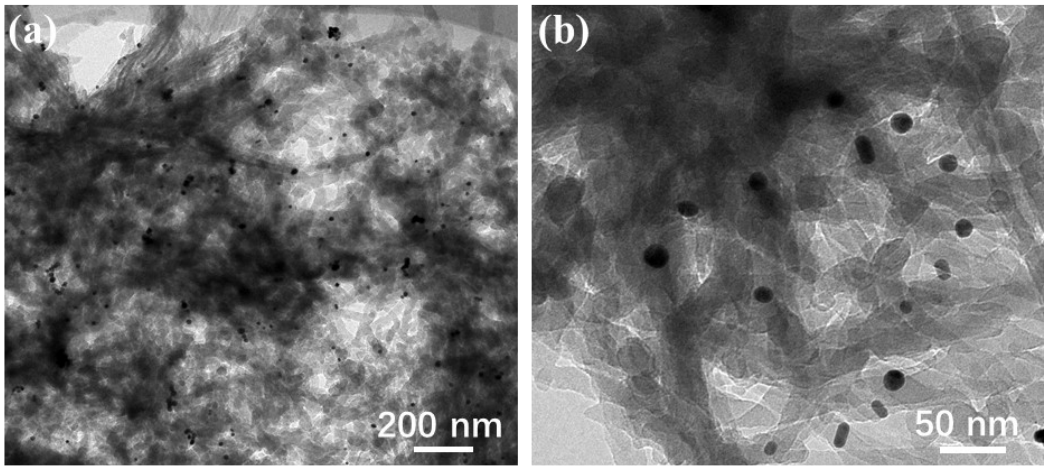

Fig. S6 TEM images of Au-COF at different magnification.

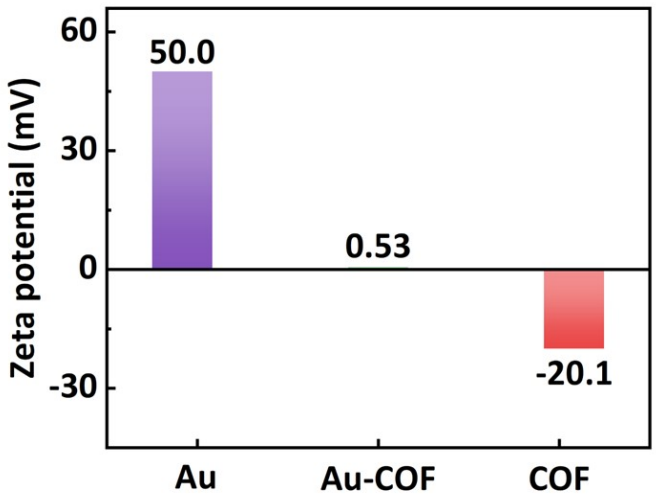

Fig. S7 Zeta Potential of various materials.

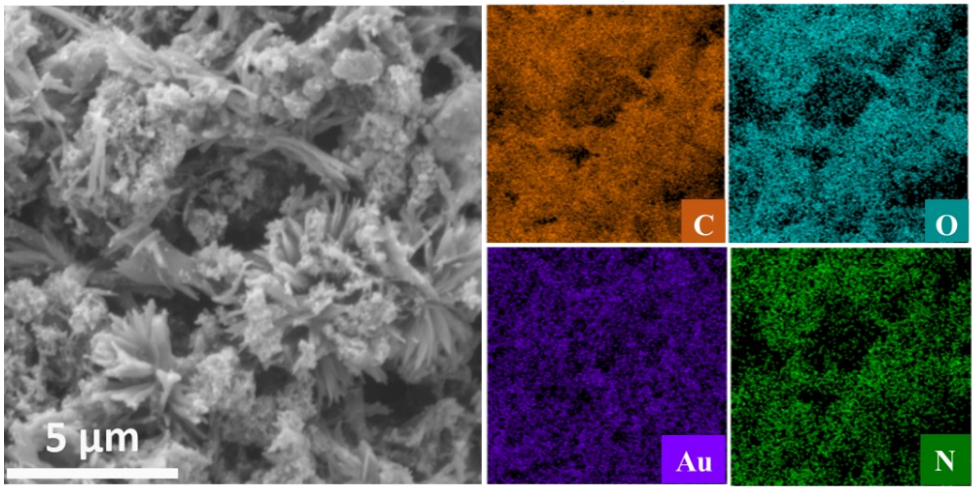

Fig. S8 SEM and corresponding elemental mapping images of Au-COF/rGO powder.

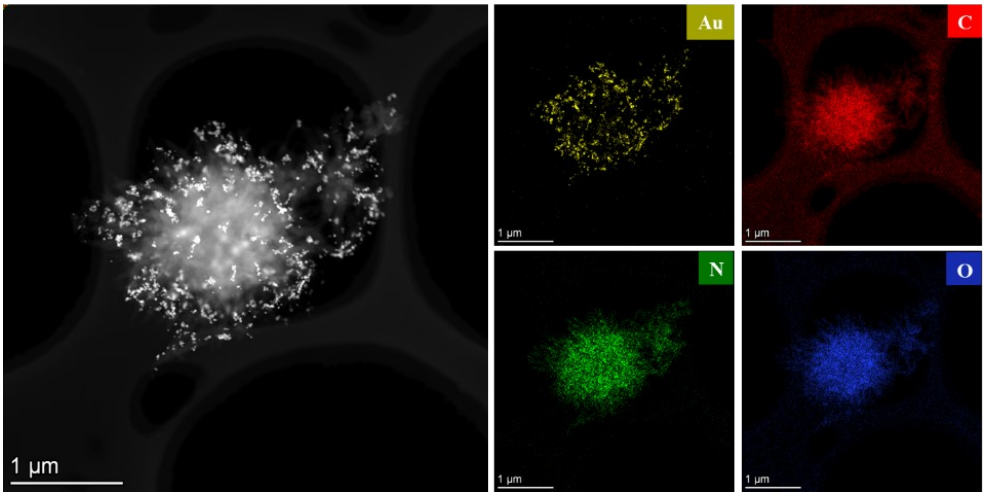

Fig. S9 TEM and corresponding elemental mapping images of Au-COF/rGO powder.

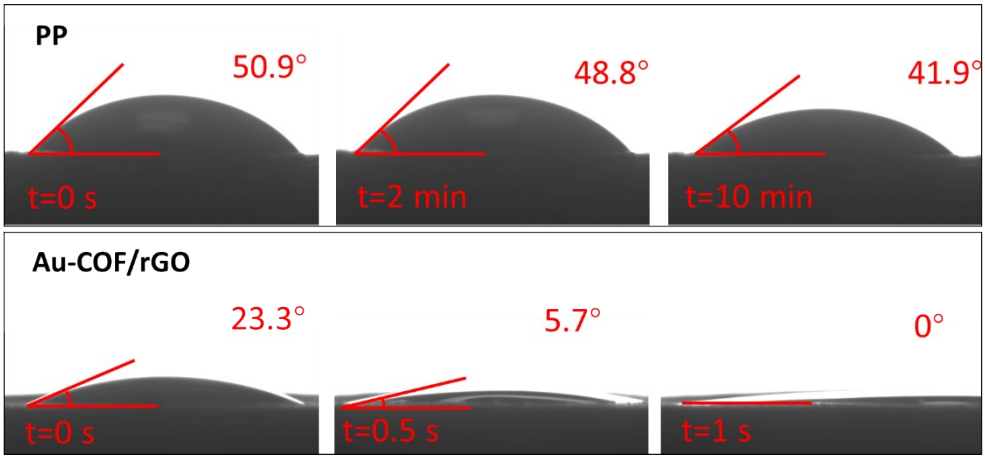

Fig. S10 Photographs of static liquid electrolyte contact angles of different separators at different rest time. 1 M LiTFSI with 2 wt% $LiNO_3$ in DOL/DME (v/v=1:1) was used as a liquid electrolyte.

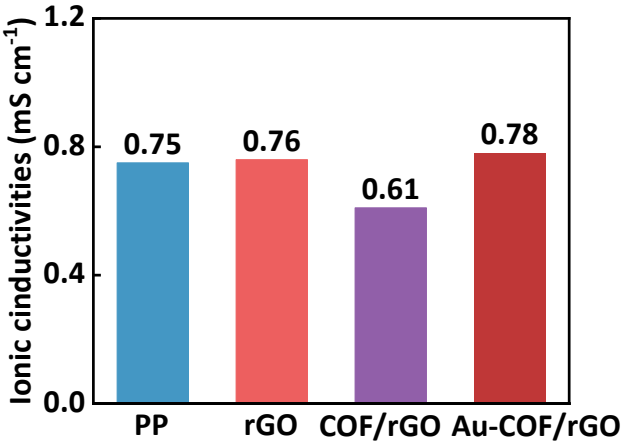

Fig. S11 Li ion conductivity of symmetric cells with various separators.

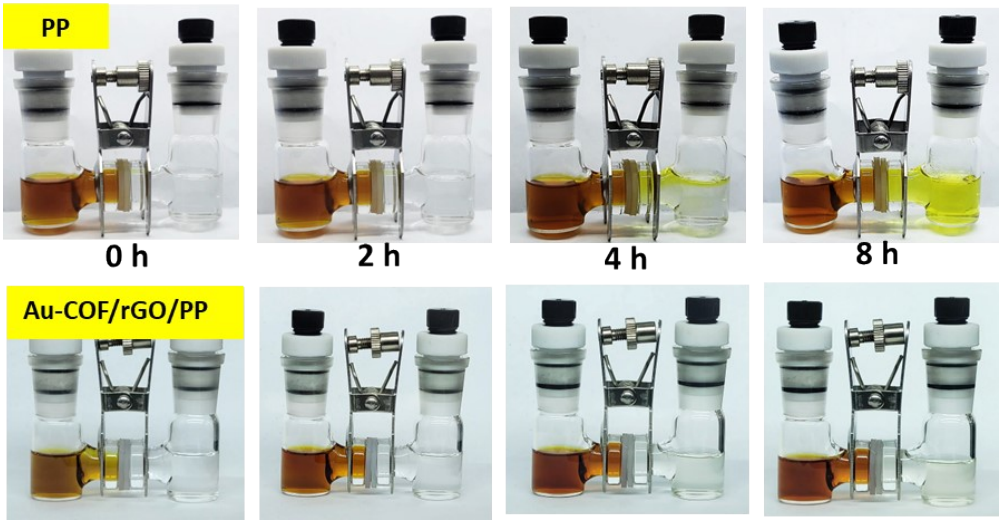

Fig. S12 Permeation experiments. Digital photographs of H-type devices with original PP separator and Au-COF/rGO coated PP separator. The inside of left chamber is Li_2S_6 in DOL/DME (v/v=1:1) solution, while the inside of right chamber is the pure DOL/DME (v/v=1:1) solvent.

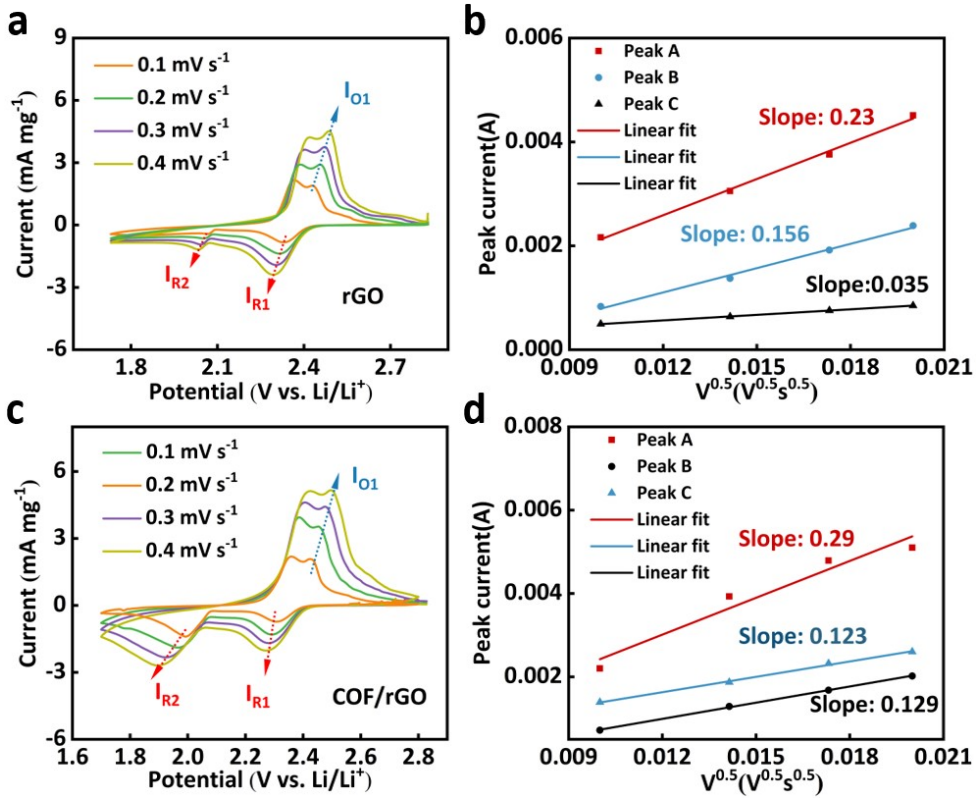

Fig. S13 CV curves at different scan rates and the corresponding linear fits of the peak current of the cells with the (a, b) rGO and (c, d) COF/rGO separators.

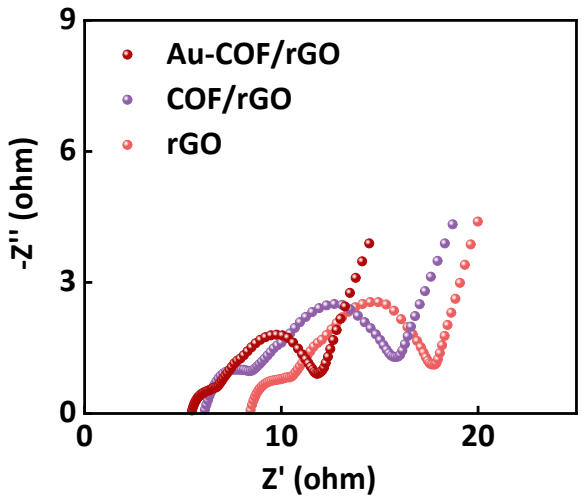

Fig. S14 EIS curves of Au-COF/rGO, COF/rGO and rGO symmetry cells.

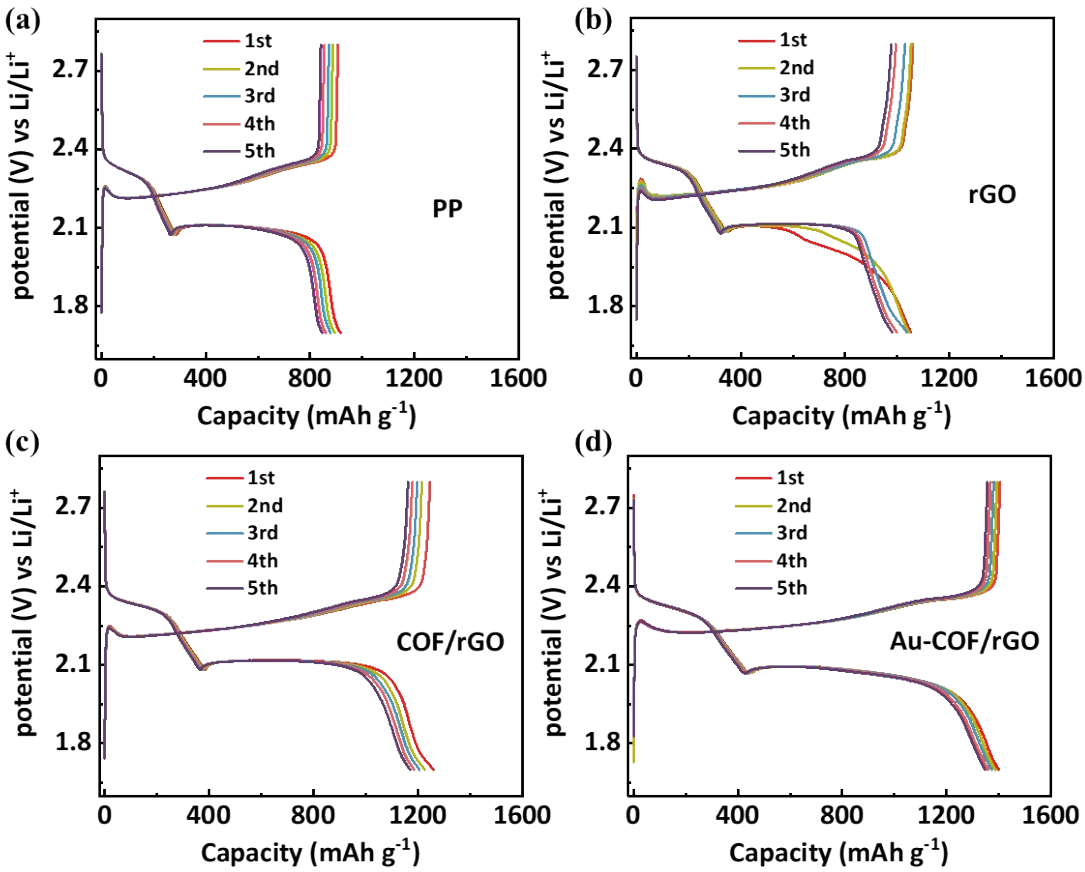

Fig. S15 First five charge-discharge curves of the Li-S batteries with various separators at 0.2 C.

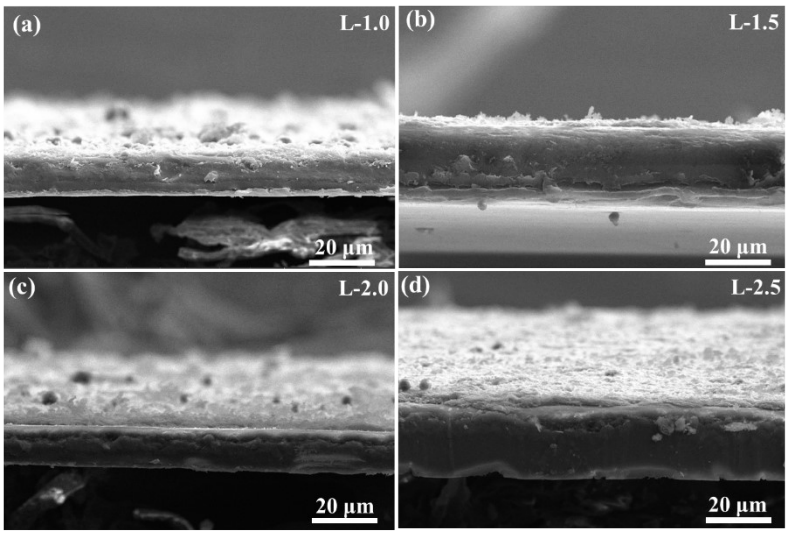

Fig. S16 Side-view SEM images of the Au-COF/rGO layer with different thickness, which was constructed by adjusting the total loading amount of the three components based on the mass ratio of Au: COF: rGO=1: 1: 1. The loading amount of Au: COF: rGO: (a) 1.0 mg: 1.0 mg: 1.0 mg; (b) 1.5 mg: 1.5 mg: 1.5 mg; (c) 2.0 mg: 2.0 mg: 2.0 mg; (d) 2.5 mg: 2.5 mg: 2.5 mg.

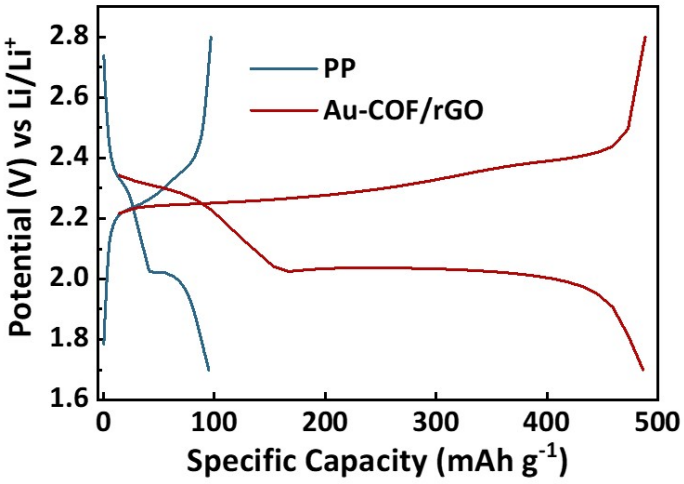

Fig. S17 Charge-discharge voltage profiles of Li-S cells with different interface after 1000 cycles.

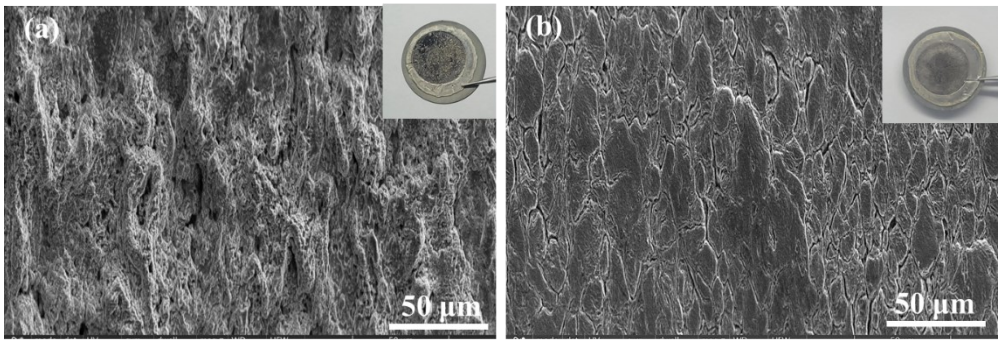

Fig. S18 SEM images of Li metal anode after cycling in the Li-S cells with different interface: (a) PP; (b) Au-COF/rGO. The inset presents a corresponding digital photo of Li metal anode.

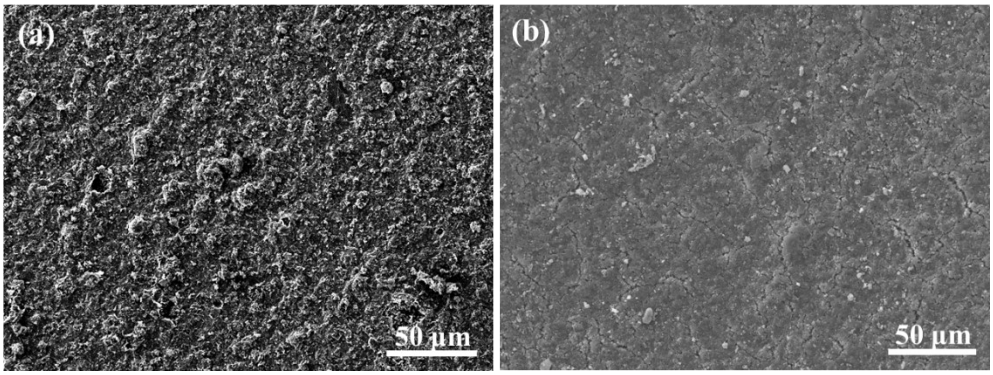

Fig. S19 SEM images of Au-COF/rGO **a** before and **b** after cycling.

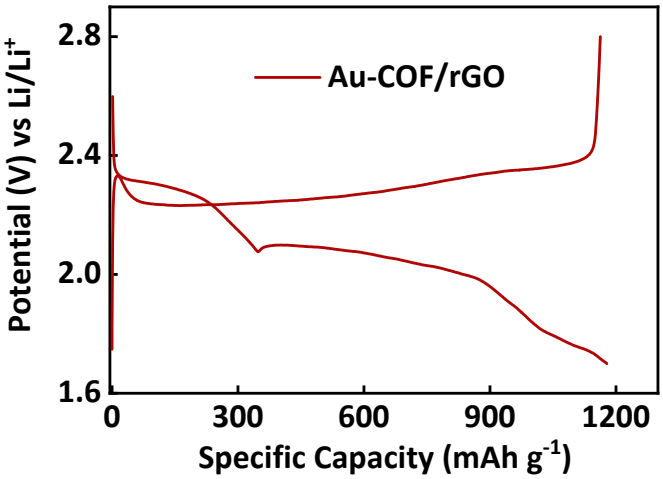

Fig. S20 Charge-discharge voltage profiles at 0.1 C of Au-COF/rGO-based Li-S cell with a high sulfur loading of 3.7 mg cm^{-2}.

Table S1 Li^+ diffusion coefficients of various separators.

Separator	D_{Li+} at peak A [$cm^2\ s^{-1}$]	D_{Li+} at peak B [$cm^2\ s^{-1}$]	D_{Li+} at peak C [$cm^2\ s^{-1}$]
PP	6.3×10^{-8}	1.9×10^{-8}	9.5×10^{-9}
rGO/PP	1.0×10^{-7}	4.7×10^{-8}	2.4×10^{-9}
COF/rGO/PP	1.6×10^{-7}	2.9×10^{-8}	3.2×10^{-8}
Au-COF/rGO/PP	2.3×10^{-7}	3.3×10^{-8}	2.9×10^{-8}

Table S2 Discharge specific capacity of the Li-S cells with different mass rations of Au decorated COF/rGO interface.

Separator	Original capacity (mA h g^{-1})	Capacity after 500 cycles (mA h g^{-1})	Capacity decay rate (%)
0.5Au-COF/rGO	1204	458	0.124
1.0Au-COF/rGO	1221	719	0.082
1.5Au-COF/rGO	1265	515	0.119
2.0Au-COF/rGO	1135	452	0.120

Table S3 Discharge specific capacity of the Li-S cells with Au-COF/rGO interface in different thicknesses based on the mass ratio of Au: COF: rGO=1: 1: 1.

Separator	Original capacity (mA h g^{-1})	Capacity after 500 cycles (mA h g^{-1})	Capacity decay rate(%)
L-1.0	1094	458	0.162
L-1.5	1221	719	0.082
L-2.0	1137	536	0.163
L-2.5	883	369	0.163

Table S4 The comprehensive comparison of the electrochemical performance of Li-S cells with various interface/separators.

Separator	Max Capacity (mA h g^{-1})	Rate Capacity (mA h g^{-1})	Cycling Performance			Reference
			Rate	Cycle Number	Capacity Fading Rate/Cycle	
SCOF-2	1219 (0.1 C)	470 (5 C)	1 C	800	0.047%	S1
S/D-[4+3]COFs2-3	1350 (0.1 C)	632 (2.5 C)	0.5 C	500	0.03%	S2
Li-CON@GN/Celgard	1622 (0.1 C)	782 (4 C)	1 C	600	0.057%	S3
COF-1 NN	1120 (0.2 C)	580 (10 C)	2 C	300	0.053%	S4
R-COF-BTD@S	1600 (0.1 C)	700 (2 C)	0.5 C	200	0.012%	S5
TPB-DMTP-COF	880 (0.5 C)	480 (2.5 C)	1 C	800	0.05%	S6
TpPa-SO_3Li/CNT/Celgard	1590 (0.1 C)	610 (4 C)	4 C	400	0.039%	S7
TpPa–SO_3H@PP	1290 (0.1 C)	490 (4 C)	1 C	500	0.05%	S8
CTP-1	1500 (0.05 C)	600 (5 C)	1 C	800	0.048%	S9
Au-COF/rGO	1420 (0.2 C)	568 (4 C)	1 C	1000	0.047%	This work

Table S5 The comprehensive comparison of the electrochemical performance of Li-S cells with various functional interface/separators at high sulfur loading.

Separator	Cycling Performance					Reference
	Rate (C)	Max Capacity (mA h g^{-1})	Cycle Number	Sulfur loading (mg cm^{-2})	Capacity Fading Rate/Cycle	
SCOF-2	0.2	855	100	3.2	82.5%	S1
TpPa–SO_3H@PP	0.2	800	100	5.0	75.0%	S8
COF-TPT(OH)@S	0.1	1080	10	5.0	90.1%	S10
COF-MF@S	0.2	905	150	3.7	80.3%	S11
COF-PDA/SWCNT	0.1	922	60	4.5	75.5%	S12
4F-COF	0.05	844	200	9.0	74.0%	S13
S/D- [4+3] COFs2-3	0.5	795	50	4.0	74.0%	S14
COF66	0.2	1015	100	3.6	76.5%	S15
Au-COF/rGO	0.1	1162	50	3.7	82.8%	This work

Supporting References

S1. J. Xu, S. An, X. Song, Y. Cao, N. Wang, X. Qiu, Y. Zhang, J. Chen, X. Duan and J. Huang, Adv. Mater., 2021, **33**, 2105178.

S2. Q. Wang, K. Tang, Q. Liao, Y. Xu, H. Xu, Y. Wang, P. Wang, Z. Meng and K. Xi, Adv. Funct. Mater., 2023, **33**, 2211356.

S3. Y. Cao, C. Liu, M. Wang, H. Yang, S. Liu, H. Wang, Z. Yang, F. Pan, Z. Jiang and J. Sun, Energy Stor. Mater., 2020, **29**, 207-215.

S4. J. Yoo, S.-J. Cho, G. Y. Jung, S. H. Kim, K.-H. Choi, J.-H. Kim, C. K. Lee, S. K. Kwak and S.-Y. Lee, Nano Lett., 2016, **16**, 3292-3300.

S5. Y. Ge, Y. Meng, L. Liu, J. Li, X. Huang and D. Xiao, Green Energy Environ., 2023.

S6. Y. Yang, X.-J. Hong, C.-L. Song, G.-H. Li, Y.-X. Zheng, D.-D. Zhou, M. Zhang, Y.-P. Cai and H. Wang, J. Mater. Chem. A, 2019, **7**, 16323-16329.

S7. Y. Cao, H. Wu, G. Li, C. Liu, L. Cao, Y. Zhang, W. Bao, H. Wang, Y. Yao and S. Liu, Nano Lett., 2021, **21**, 2997-3006.

S8. J. Zhao, G. Yan, X. Zhang, Y. Feng, N. Li, J. Shi and X. Qu, Chem. Eng. J., 2022, **442**, 136352.

S9. J. Xu, F. Yu, J. Hua, W. Tang, C. Yang, S. Hu, S. Zhao, X. Zhang, Z. Xin and D. Niu, Chem. Eng. J.., 2020, **392**, 123694.

S10. Y. Ge, J. Li, Y. Meng and D. Xiao, Nano Energy, 2023, **109**, 108297.

S11. X. Hu, J. Jian, Z. Fang, L. Zhong, Z. Yuan, M. Yang, S. Ren, Q. Zhang, X. Chen and D. Yu, Energy Stor. Mater., 2019, **22**, 40-47.

S12. L. Han, Y. Yang, S. Sun, J. Yue and J. Li, ACS Sustain. Chem. Eng., 2023.

S13. K. Zhang, X. Li, L. Ma, F. Chen, Z. Chen, Y. Yuan, Y. Zhao, J. Yang, J. Liu and K. Xie, ACS Nano, 2023, **17**, 2901-2911.

S14. Q. Wang, K. Tang, Q. Liao, Y. Xu, H. Xu, Y. Wang, P. Wang, Z. Meng and K. Xi, Adv. Funct. Mater., 2023, **33**, 2211356.

S15. J. Xu, W. Tang, C. Yang, I. Manke, N. Chen, F. Lai, T. Xu, S. An, H. Liu and Z. Zhang, ACS Energy Lett., 2021, **6**, 3053-3062.